Organic & Biomolecular Chemistry

PAPER

View Article Online
View Journal | View Issue

Cite this: *Org. Biomol. Chem.*, 2014, **12**, 1488

Identification and optimization of short helical peptides with novel reactive functionality as catalysts for acyl transfer by reactive tagging†

Silvia Bezer,[a] Masaomi Matsumoto,[a] Michael W. Lodewyk,[b] Stephen J. Lee,[c] Dean J. Tantillo,[b] Michel R. Gagné*[a] and Marcey L. Waters*[a]

Received 10th July 2013,
Accepted 9th January 2014

DOI: 10.1039/c3ob41421c

www.rsc.org/obc

Herein we describe the screening and subsequent optimization of peptide catalysts for ester activation. A combinatorial methodology using dye-tagged substrate analogs is described for determining which components of a His-containing helical library display acyl transfer activity. We found that helical peptides display high activity, and amino acids that reinforce this propensity are advantaged. Through this approach two new structural motifs have been discovered that are capable of activating esters in organic solvents. Unlike most acyl transfer catalysts functioning in organic solvents, these catalysts are histidine- rather than *N*-alkyl histidine-based. Longer peptides with localization of reactive groups on the C-terminal end of the peptide were found to further enhance catalytic activity up to ~2800-fold over background.

Introduction

Minimalist peptide catalysts have long been a goal of chemists seeking solutions to practical problems in organic synthesis and to bio-organic chemists seeking to understand how inherently complex enzymes can be simplified to identify their key catalytic features. The tension between this reductionist push and the pull of massive structural diversity in polypeptides has necessarily forced the field towards screening techniques that enable one to competitively assay, in parallel, individually encoded library members in one-bead one-peptide format.[1–5] At the outset of our own studies we wished to test a hybrid screening protocol for the discovery of biomimetic imidazole-based acyl transfer catalysts that functioned in organic solvents. This methodology began with a mechanism-based analysis of the two-step nucleophilic acylation of an alcohol substrate (Scheme 1). Since k_1 is typically rate limiting in the presence of imidazole,[6] we considered the possibility that nucleophilic catalysts could be discovered by examining

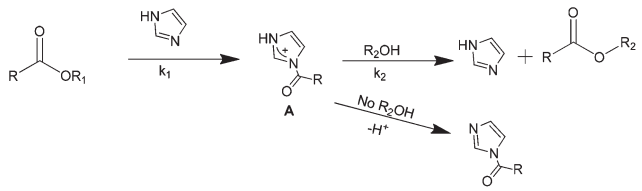

Scheme 1 Transesterification reaction catalyzed by imidazole and reactive tagging strategy.

His-containing peptide libraries. In a competitive assay for a limited quantity of a dye-tagged active ester, the absence of a nucleophile would prevent k_2, thus tagging those His-peptides with the largest k_1 for subsequent identification. The de Clercq group, in particular, has followed a similar course for the identification of peptides that accelerate serine O-acylation, though a mention of reversible histidine N-acylation is made.[7–9]

The focus of our efforts was on peptide secondary structures that maximized our ability to convert peptide hit sequences into active site structures that reliably position critical side-chains into 3-dimensional space. Short peptides that take on helical structure in organic solvent (α-helix and/or 3_{10}-helix) were selected as the scaffold because the variable $i + 3/i - 3$ and $i + 4/i - 4$ positions in the linear sequence place functionality in close proximity to the *i*-position, to which a histidine (His) residue was placed (Fig. 1). As will be discussed, this strategy enables optimization of the helical scaffold and the discovery of several previously unidentified functional group assemblies for accelerating acyl transfer reactions.[10–16]

[a]*Department of Chemistry, University of North Carolina at Chapel Hill, Chapel Hill, North Carolina 27599-3290, USA. E-mail: mgagne@unc.edu, mlwaters@unc.edu*
[b]*Department of Chemistry, University of California-Davis, Davis, California 95616, USA*
[c]*U.S. Army Research Office, P.O. Box 12211, Research Triangle Park, North Carolina 27709, USA*

†Electronic supplementary information (ESI) available: Peptide and peptide-library synthesis, peptides' mass-spectrograms, reactive tag synthesis and their physical data, library hits mass-spectrograms, CD spectra, NOE spectra, cartoon representations of peptide structures, kinetic details plots, computational work. See DOI: 10.1039/c3ob41421c

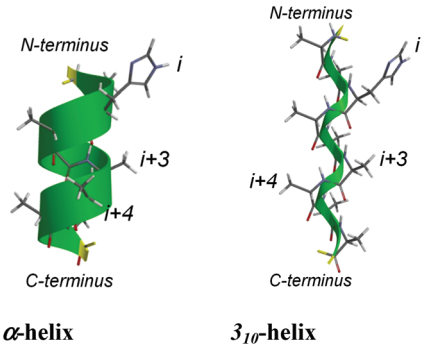

Fig. 1 Spartan generated model for α- and 3_{10}-helices based on a poly-alanine/His 9-mer peptide showing the relative positions of *i*, *i* + 3, and *i* + 4 residues in the helix.

The viability of the described approach is validated by the identification of new non-biological catalytic moieties that function in non-aqueous solvents.[12,13,15]

Results and discussion

Library synthesis and screening procedure

Based on the above criteria, a library of helical imidazole-containing peptides was synthesized on solid support. The library was prepared on amino functionalized Tentagel resin with a standard photo-cleavable linker following the protocol for split-and-mix synthesis (see ESI†).[17–19] To guard against selecting hits that were influenced by the dye-component or the leaving group, four dye-labeled active esters were used **RT1–4** (Fig. 2). These differ as follows: **RT1** is the succinimide ester of Disperse Red 1; **RT2** is the *p*-nitrophenyl ester of Disperse Red 1;[7–9] **RT3** is the *p*-nitrophenyl ester of Disperse Red 1 separated by a linker; and **RT4** is the succinimide ester of Bodipy plus linker. The expected relative activity of these esters is: **RT1** > **RT2** > **RT4** > **RT3** based on known reactivities of succinimidyl esters relative to nitrophenyl esters coupled with differences in inductive effects of the linkers between the ester group and dye.[20]

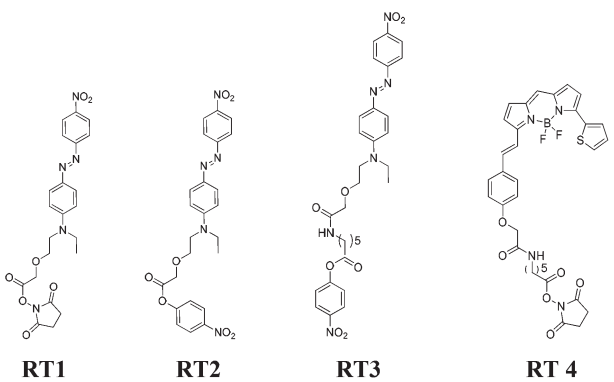

Fig. 2 Reactive tags **RT1–4** for library screening.

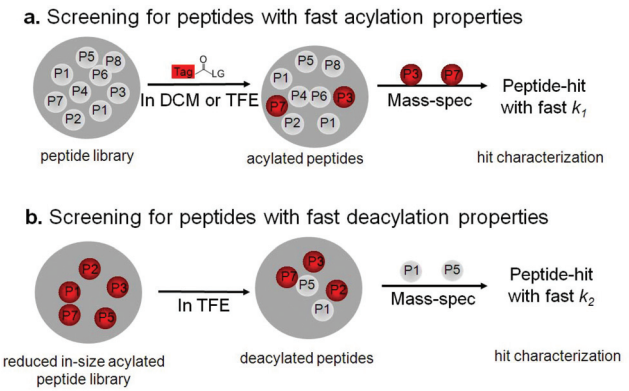

Fig. 3 Two-step screening procedure for discovering the most reactive peptide-catalysts.

The screening was achieved by exposing Tentagel resin beads containing His-peptides to a dichloromethane (DCM) or trifluoroethanol (TFE) solution of the reactive tag until approximately 1% of the beads were visibly colored. It is these beads which should contain the most reactive peptides (Fig. 3a). The reactive tagging scheme leads to a subset of beads that are intensely red in the case of Disperse Red 1-taggents **RT1–3** and blue for Bodipy-based agent **RT4**. Control experiments with (i) acetylated Tentagel resin, (ii) N-terminus capped polyalanine peptide containing no His on Tentagel, and (iii) N-terminus capped Trt protected-His/polyalanine peptide on Tentagel, established that binding/coloration does not occur without a reactive imidazole. Hit precision was established *via* duplicate or triplicate runs and each peptide hit was identified by MALDI MS analysis of the photolytically cleaved product in MeOH (see ESI†).[8] In the case of ambiguous MS assignments, the candidates were resynthesized and screened independently. This screening procedure identifies members of the library with rapid N-acylation rates (k_1 in Scheme 1).

Information on the competitive rate of library *deacylation* was obtained by carrying out a second screening on the colored beads, those that previously displayed a competitive k_1 step (Scheme 1). This was accomplished by pooling the dye-tagged beads from the first screening (library **L3** only, *vide infra*) and exposing them to deacylation conditions (added TFE) while now searching for those with rapid bleaching kinetics (Fig. 3b). This 2-round screening procedure is similar to that reported by De Clercq, who sought catalysts functioning by a serine acylation mechanism.[8]

Peptide-catalyst structure optimization

The strong α-helix preference of polyalanine led us to initiate our study with sequences rich in Ala.[21–26] Because Ala-rich peptides have been shown to increase their helicity in organic solvents, such as TFE, a 9-residue scaffold was selected corresponding to two full α-helical turns as the basis of the library.[27,28] Library 1, **L1**, had His at the *i*-residue and 34 variable substituents at the *i* + 3 position (Charts 1 and 2). The

L1 Ac-AA**H**AA**X**AAA-NH_2

L2 Ac-**X**A**YXXXYX**A-NH_2

L3 Ac-BA**H**AB**XY**BA-NH_2

Chart 1 Amino acid sequence for libraries L1–L3.[a] a. In L1 and L3, X and Y are shown in Chart 2. In L2, X corresponds to either Aib or Ala; Y corresponds to His, Aib, or Ala.

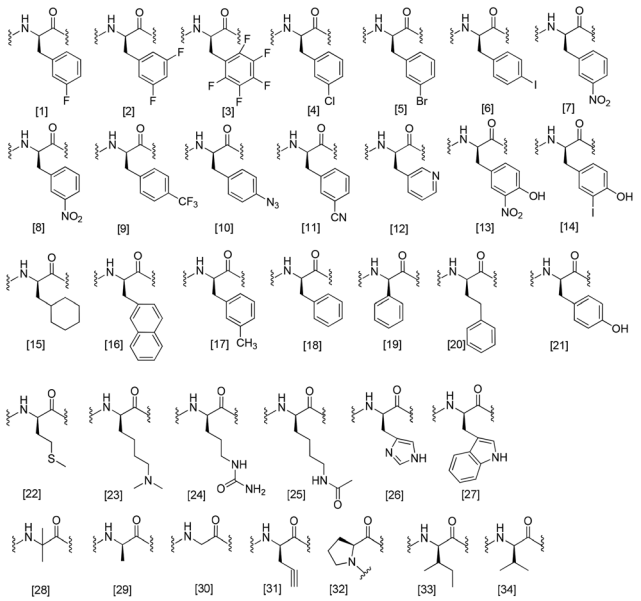

Chart 2 Amino acids at variable positions in libraries L1 and L3.

i/*i* + 3 relationship strategically places these two positions in close proximity regardless of whether the individual peptide adopted an α- (3.6 residues per turn) or 3_{10}-helix (3 residues per turn).

The variable position explored how H-bond donors and acceptors, aromatic groups and residues imposing conformational biases influenced the rate of tagging (Chart 2). Potential nucleophilic residues that could interfere with His acylation were excluded. As expected, the rate of library tagging depended on the activity of each reactive tag with **RT1–RT3** taking 25 s, 5 min, and 3 h, respectively to tag ~1% of the beads. MS analysis of the photo-cleaved colored beads (in MeOH) indicated that a single unique peptide (**Hit1**) was identified from this library (2.8% of total), whose molecular weight identified it as Ac-AA**H**AA**B**AAA-NH_2 (**A_7HB**, X = B, aminoisobutyric acid or Aib, [28] in Chart 2) (Fig. S2a†). Importantly, although Aib does not contain potentially reactive functional groups, it is a strong promoter and stabilizer of helicity in short peptides.[29,30]

These results led to the design of a second-generation library, **L2** (Chart 1), whose goal was determining an optimum backbone sequence for high inherent activity. Since the number and positioning of the Aibs within a poly-Ala sequence influences both the absolute helicity and helical conformation,[30] **L2**, an 8 membered library, sought to determine

Hit2a Ac-**B**A**H**A**B**AA**B**A-NH_2 **(His-scaffold 2T)**

Hit2b Ac-**B**A**B**AA**H**AAA-NH_2

Chart 3 Amino acid sequence for the identified hits in the library **L2**.

whether the Aib effect was localized to the *i* + 3 position or if other positions or stabilization schemes might lead to improved tagging activity. Library screening identified two high activity peptides (Chart 3), one containing three Aib residues, **Hit2a**, and a second containing two Aib residues, **Hit2b**; both contain an N-terminal Aib. As discussed below, both sequences similarly fold into a hybrid 3_{10}/α-helix, which is common for peptides of similar length and Aib content.[30] **Hit2a** was chosen for further investigation as it allows the positioning of variable residues in the *i* + 3 and *i* + 4 positions without altering the number of Aib residues in the peptide.

Scaffold-optimized library generation and screening

A 425-member third-generation library **L3** was constructed on the **Hit2a** scaffold (**His-scaffold 2T**, where 2T indicates two turns) by independently varying the *i* + 3 (with X) and the *i* + 4 (with Y) positions (Charts 1 and 2). Screening of **L3** in DCM with reactive tags **RT2–RT4** selected a single peptide (~0.2% of **L3**) that was independent of the reactive tag type. Other peptides were identified with the various reactive tagging agents, but only **Hit3a** was observed in *each* screen. Its MW (Fig. S2b–d†) was consistent with X = citrulline (Cit, [24] in Chart 2) and Y = 3-pyridylalanine (3Py, [12] in Chart 2), giving **His-3PyCit 2T** (Fig. 4). Repeating the screen in TFE with **RT3** again selected for **His-3PyCit 2T**, indicating that the hit was robust and superior in multiple solvents (Table S1 and Fig. S2e†). **His-3PyCit 2T** therefore has the highest k_1 rate in **L3**. More importantly its high rate holds for different leaving groups, and is independent of dye structure and solvent (DCM and TFE). Its arrangement of functional groups represents a unique, non-biological structural motif for accelerating acyl activation reactions in organic solvents.

Library **L3** was also subjected to a two-step screening protocol with reactive tag **RT2** to look for hits that additionally have competitive deacylation properties. In this mode, the tagging time was extended so that ~10% of the most reactive beads became colored in DCM. These red beads were removed from the library and subjected to a deacylation screen by the

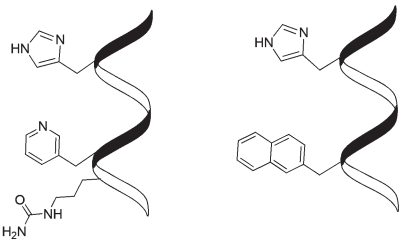

Hit 3a: His-3Py-Cit 2T **Hit 3b: His-2Nal-Gly 2T**

Fig. 4 Cartoon representation of the hits from library **L3**.

addition of TFE and looking for *bleaching* of the beads. In principle, beads displaying a fast k_1 (acylation) and a competent deacylation (k_3) should have good catalytic properties. This two step treatment of **L3** led to a single peptide corresponding to X = 2-naphthylalanine (2Nal residue [16] in Chart 2), Y = glycine (G, residue [30] in Chart 2), (**His-2Nal-Gly 2T**, Fig. 4). The peptide de-tagging rates were slower than the tagging, requiring 2 h to identify the first bleached beads. Like the single-step screening, the 2Nal/Gly combination is a unique structural motif for accelerating the acyl transfer reaction.

Assessment of catalytic efficiency

The compounds identified in the course of screening **L3** were next examined in solution using 4-nitrophenyl 2-methoxyacetate in TFE (Scheme 2). The progress of the acyl transfer was monitored by UV-Vis spectroscopy watching the growth of 4-nitrophenol at 320 nm using 10 mol% of the catalyst. A slow background rate was observed for the reaction of the ester in TFE, and this was assigned a relative rate of 1. The initial rates using **His-3Py-Cit 2T** and **His-2Nal-Gly 2T** were 660- (Table 1, entry 2) and 240-fold (Table 1, entry 3) greater than background, respectively, verifying that both tagging hits efficiently catalyze acyl transfer to TFE.

The unique functional motif of **His-3Py-Cit 2T** was probed through a variety of methods, including an "alanine scan" to test peptides lacking one or two of the three key groups: (a) no 3-pyridylalanine (**His-Ala-Cit 2T**, entry 4, Table 1); (b) no citrulline (**His-3Py-Ala 2T**, entry 5); (c) no imidazole (**Ala-3Py-Cit 2T**, entry 7); (d) removal of both the 3-Py and Cit groups (**His-scaffold 2T**, entry 1). Each of these variants in addition to *N*-methylated His (**MeHis-3Py-Cit 2T**, entry 6) were slower, indicating a synergistic arrangement of the functional groups.

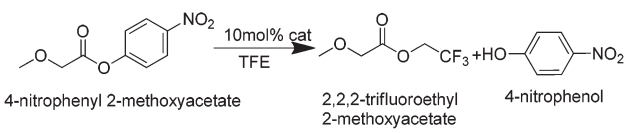

Scheme 2 4-Nitrophenyl 2-methoxyacetate (20 mM) and 10 mol% catalyst in TFE at 25 °C.

Since helical propensity should increase with increasing peptide length several variants were examined including a 4-turn **His-3Py-Cit 4T** (entry 9) and a 4-turn **His-2Nal-Gly 4T** (entry 14); each showed significant increases in their initial k_{rel} rates of 2800- and 2200-fold, respectively (Table 1). These 4-turn analogs represent the best catalysts in this series.

When the active site residues of **His-3Py-Cit 4T** were moved to the N-terminus or their order was reversed (**His-3Py-Cit mid 4T** (entry 12) and **Cit-3Py-His 4T** (entry 13), respectively), less active catalysts were obtained. The helix C-terminus thus creates a microenvironment more conducive to catalysis, perhaps due to differences in fraying and in side chain orientation.

The pyridyl isomers of **His-3Py-Cit 4T** were also investigated. When the basic nitrogen was shifted to the *ortho*-position (**His-2Py-Cit 4T**, entry 10) a catalyst of similar activity was realized, though moving N to the *para*-position (**His-4Py-Cit 4T**, entry 11) significantly impeded catalysis relative to the parent structure.

The acyl transfer reaction in Scheme 2 was also followed by ^{1}H NMR spectroscopy. Fig. 5a shows the complete time course of the reaction catalyzed by 10 mol% **His-3Py-Cit 4T**. Consumption of ester is roughly first order (see Fig. S4a†) and the overall transformation is free of induction periods. In the ^{1}H NMR spectrum no shifting of the 3-pyridyl ring resonances were noted. However, chemical shift changes for the imidazole CHs indicated that imidazole protonation accompanies the conversion (to ~25%, Fig. 5b). A nucleophilic mechanism for acyl transfer suggests that partial protonation of imidazole would be deactivating, and might explain the slight slowing in the first-order plot. Partial protonation of His-containing peptides could be recapitulated by the sequential addition

Table 1 Initial rate measured for the peptide-catalyzed trans-esterification reaction in TFE-d_3 at 25 °C

Entry	Catalyst[a]	Aligned peptide sequence[b]	Initial rate (10^{-4} mM s^{-1})	k_{rel}[c]	R[d]
1	**His-scaffold 2T**	Ac-BA**H**••ABA•••A•••BA-NH_2	0.70 ± 0.18	200	0.54
2	**His-3Py-Cit 2T**	Ac-BA**H**••AB**3Py**•**Cit**•BA-NH_2	2.64 ± 0.18	660	0.66
3	**His-2Nal-Gly 2T**	Ac-BA**H**••AB**2Nal**G•••BA-NH_2	0.93 ± 0.04	240	ND
4	**His-Ala-Cit 2T**	Ac-BA**H**••AB**A**•••**Cit**•BA-NH_2	0.67 ± 0.20	170	0.56
5	**His-3Py-Ala 2T**	Ac-BA**H**••AB**3Py**•**A**•••BA-NH_2	1.38 ± 0.22	350	0.60
6	**MeHis-3Py-Cit 2T**	Ac-BA**MeH**AB**3Py**•**Cit**•BA-NH_2	1.75 ± 0.18	440	0.62
7	**Ala-3Py-Cit 2T**	Ac-BA**A**••AB**3Py**•**Cit**•BA-NH_2	0.08 ± 0.01	20	ND
8	**His-scaffold 4T**	Ac-BAA••B••AABA**H**••A••BA••A••BA-NH_2	3.03 ± 0.65	760	0.66
9	**His-3Py-Cit 4T**	Ac-BAA••B••AABA**H**••A••B**3PyCit**BA-NH_2	11.03 ± 0.47	2800	0.72
10	**His-2Py-Cit 4T**	Ac-BAA••B••AABA**H**••A••B**2PyCit**BA-NH_2	9.92 ± 0.56	2500	0.69
11	**His-4Py-Cit 4T**	Ac-BAA••B••AABA**H**••A••B**4PyCit**BA-NH_2	3.60 ± 0.30	900	0.74
12	**His-3Py-Cit mid 4T**	Ac-BAA••B••A**H**AB**3PyCit**BA•••A•BA-NH_2	5.20 ± 0.30	1300	0.78
13	**Cit-3Py-His 4T**	Ac-AB**Cit3Py**BA**H**AB••A••AB•••A•BA-NH_2	2.39 ± 0.08	600	0.71
14	**His-2Nal-Gly 4T**	Ac-BAA••B••AABA**H**••A••B**2Nal**G•BA-NH_2	8.95 ± 0.79	2200	ND

[a] See the cartoon representation of the peptide structures in Fig. S3. [b] Dots are included to align the peptide sequences. [c] The initial rate for the uncatalyzed reaction for the acylation of TFE-d_3 is 4×10^{-7} mM s^{-1}, and is assigned a relative rate of 1. [d] R value characterizes the type of helix, where $R = [\Theta]_{222}/[\Theta]_{205}$ (see Peptide structure section).

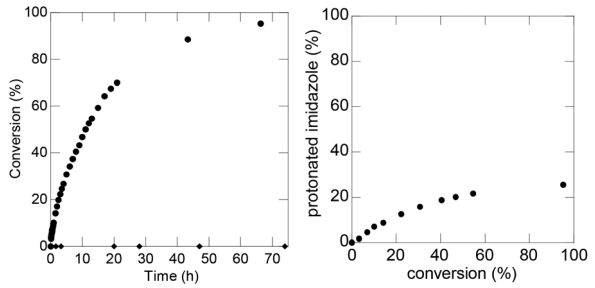

Fig. 5 Kinetic assay of the peptide-catalyst in TFE-d_3 in 20 mM substrate and 10 mol% catalyst monitored by ^{1}H-NMR. (a): (◆) no catalyst (●) **His-3Py-Cit 4T**; (b) imidazole protonation determined from $\Delta\delta$ of the δCH protons of imidazole for **His-3Py-Cit 4T**.

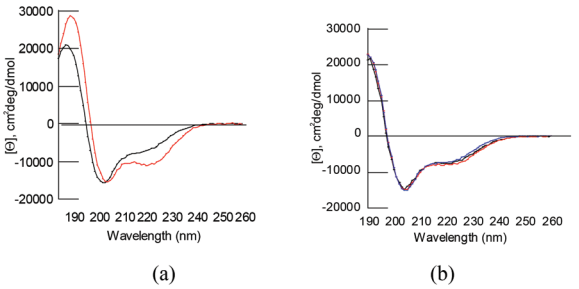

Fig. 6 CD spectra of 0.2 mM peptide solutions in TFE at: (a) 4 °C; **Ala$_8$His** (black), **Ala$_7$HisAib** (red); (b) 25 °C; **Ala-scaffold 2T** (black), **Hit 2a** (**His-scaffold 2T**) (red), **Hit 2b** (blue).

Ala$_8$His	Ac-AAHAAAAAA-NH$_2$
Ala$_7$HisAib (Hit1)	Ac-AAHAABAAA-NH$_2$
Ala-scaffold 2T	Ac-BAAABAABA-NH$_2$

Chart 4 Sequence of the Ala-based peptides.

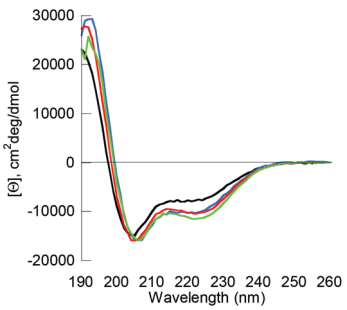

Fig. 7 CD spectra of 0.2 mM peptide solutions in TFE at 25 °C; **His-scaffold 2T** (black), **His-3Py-Cit 2T** (blue), **His-scaffold 4T** (red), **His-3Py-Cit 4T** (green).

of 4-nitrophenol to the peptide in the absence of ester (see Fig. S4b†).

Peptide structures in TFE by CD

To complement the catalytic properties of these peptides in TFE, their structures were probed by CD spectroscopy. The right-handed α-helix gives rise to two negative bands at 222 and 208 nm (a superposition of the random coil π–π* transition at 200 nm and the α-helix π–π* transition at 208 nm) of almost equal intensities and a strong positive band at about 192 nm.[31] The 3_{10}-helix has conformational parameters close to the α-helix, the former being slightly tighter and more elongated (Fig. 1).[32,33] One possible criterion to distinguish them is by determining the ratio of the bands $R = [\Theta]_{222}/[\Theta]_{208}$.[32,33] The α-helical peptides are known to have R values of ~1 whereas 3_{10}-helices have values near 0.4.[32,33] The CD spectrum of **Ala$_8$His**, the reference scaffold for **L1**, exhibits two negative bands at 222 and 203 nm and a positive band at 190 nm, indicating a helical structure. The ratio, R, of the 222/203 nm peaks is 0.45 suggesting a dominant 3_{10}-helix (Fig. 6a).[32,33] When **Ala$_8$His** was modified with an Aib residue in the $i + 3$ position (**Hit1** from **L1**), the resulting peptide **Ala$_7$-HisAib** (**Hit 1**) shows a greater intensity at 222 and 190 nm, with $R = [\Theta]_{222}/[\Theta]_{205} = 0.71$ (Fig. 5a) consistent with a better folded hybrid 3_{10}/α-helix.[32–34]

The scaffolds identified in the screening of **L2** (**Hit 2a** and **b**) showed nearly identical CD spectra corresponding to a hybrid 3_{10}/α-helix ($R = [\Theta]_{222}/[\Theta]_{205} = 0.54$, Fig. 6b).[32–34] Replacing His with Ala in **His-scaffold 2T** (**Hit 2a**) to give **Ala-scaffold 2T** (Chart 4) did not change the peptide conformation, supporting the notion that helicity is primarily nucleated by the Aib residue (Fig. 6b). Replacing two Ala residues with 3-pyridylalanine and citrulline to give **His-3Py-Cit 2T** results in higher α-helix content, as judged by a shift in the middle band from 204 to 206 nm, increased intensity at 222 nm and $R_{222/205}$ = 0.66 (Fig. 7).[32–34] The same feature was observed for all peptides containing 3-pyridylalanine (Table 1, Fig. S5†), independent of catalytic activity. When 3-pyridylalanine was removed (**His-Ala-Cit 2T**), the spectrum was similar to the **His-scaffold 2T** (Table 1, Fig. S5†). Thus, while 3Py increases helicity, it does not alone correlate with catalytic activity.

Increasing the length of **His-scaffold 2T** from 2- to 4-turns results in an increase in α-helical content, with $R = [\Theta]_{222}/[\Theta]_{205}$ increasing from 0.54 to 0.66 (Fig. 6b and Table 1, entries 1 and 8).[32–34] The 15-residue peptide-hit, **His-3Py-Cit 4T**, shows a smaller increase in α-helical content with respect to **His-3Py-Cit 2T**, with R increasing from a two-turn value of 0.66 to 0.72 (Fig. 7 and Table 1, entries 2 and 9). However, only small differences in R-values were observed for **His-3Py-Cit 4T** relative to the control peptides (**His-2Py-Cit 4T**, **His-4Py-Cit 4T**, **His-3Py-Cit mid 4T**, and **Cit-3Py-His 4T**, Fig. S6a† and Table 1, entries 9–13). As with the 2T peptides, the R value alone does not correlate with catalytic activity in the 4T series. The CD spectra for the **His-2Nal-Gly 2T** hit and **His-2Nal-Gly 4T** indicate a helical structure but naphthyl absorbance artifacts at 222 nm band make it difficult to estimate the type of helix (Fig. S6b†).

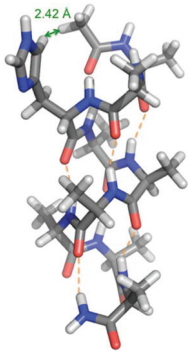

Fig. 8 Computationally determined low energy conformation for the peptide **Ala$_8$His** highlighting a possible contact between the imidazole and the *N*-acyl terminus.

Computational modeling

To better understand how the length of the peptide and/or position of the His in the helix may influence reactivity, a quantum mechanical calculation (M06-2X geometry optimization in TFE; see ESI† for details) on a model alpha-helical scaffold (**Ala$_8$His**, Chart 4) was performed (Fig. 8). A minimum energy structure was identified in which the imidazole group is in a *gauche* orientation (N–Cα–Cβ–Cγ dihedral angle = −54.5°) and the δCH proton is approximately 2.4 Å away from the capping acyl methyl group. This contact is not possible in the **His-scaffold 4T** and **His-3Py-Cit 4T** peptides, as the spacing of an extra turn between the imidazole and the N-terminus brings them outside of interaction range. Moreover, the *gauche* orientation found for Ala8His in contrast to the lowest energy conformation in an aqueous alpha-helix, which has been shown to be the *trans* conformation.[35] Interestingly, the *trans* conformation is required to bring His in close proximity to the $i + 3$ and $i + 4$ residues, suggesting that the 4T peptides may populate a more favorable conformation for catalysis than do the 2T peptides, in which His is close to the N-terminus. This is also consistent with the fact that placing 3Py and Cit at the $i - 3$ and $i - 4$ positions, respectively, (**Cit-3Py-His 4T**) results in a 4-fold decrease in reactivity (compare Table 1, entries 9 and 13). Thus, the conformation of His may be influenced by its location in the helix, which influences its catalytic activity.

Conclusions

In summary, we have found that the reactive tagging strategy used here is a promising method for identifying new catalytic functionality in on-bead peptide libraries in organic solvents. Moreover, helical peptides provide a rich environment for arranging such catalytic moieties. These studies indicate that residues that increase alpha-helicity (such as Aib) also increase catalytic efficiency. However, increased helicity alone does not account for the catalytic efficiency of the most active hits. For example, while all isomers of pyridylalanine increase alpha-helicity relative to a 3_{10} helix by about the same extent, 2- and 3-pyridylalanine provides a greater increase in catalytic efficiency than 4-pyridylalanine. Thus, based on mutation studies, 3Py and Cit both appear to be critical elements in the catalytic triad, along with His.

These studies clearly indicate the subtle influences of structure on reactivity, including the length of the helix, placement of functionality within the helix and the preference for 3_{10} or alpha-helicity. These factors would be difficult to predict, reinforcing the benefits of the screening methodology used here. While the exact catalytic roles of the 3Py and Cit sidechains have yet to be determined, this work clearly demonstrates the opportunities for discovering novel catalytic moieties using reactive tagging of helical peptide libraries and the subtle features that can influence catalytic activity.

Acknowledgements

This work was supported with funding from the Defense Threat Reduction Agency (HDTRA1-10-1-0030). M.M. acknowledges a fellowship from the NRC.

Notes and references

1 A. Berkessel, *Curr. Opin. Chem. Biol.*, 2003, **7**, 409–419.
2 K. S. Lam, M. Lebl and V. Krchnak, *Chem. Rev.*, 1997, **97**, 411–448.
3 J. D. Revell and H. Wennemers, *Curr. Opin. Chem. Biol.*, 2007, **11**, 269–278.
4 M. H. Fonseca and B. List, *Curr. Opin. Chem. Biol.*, 2004, **8**, 319–326.
5 P. Krattiger, C. McCarthy, A. Pfaltz and H. Wennemers, *Angew. Chem., Int. Ed.*, 2003, **42**, 1722–1724.
6 N. K. Pandit and K. A. Connors, *J. Pharm. Sci.*, 1982, **71**, 485–491.
7 H. De Muynck, A. Madder, N. Farcy, P. J. De Clercq, M. N. Perez-Payan, L. M. Ohberg and A. P. Davis, *Angew. Chem., Int. Ed.*, 2000, **39**, 145–148.
8 A. Madder, L. Li, H. De Muynck, N. Farcy, D. Van Haver, F. Fant, G. Vanhoenacker, P. Sandra, A. P. Davis and P. J. De Clercq, *J. Comb. Chem.*, 2002, **4**, 552–562.
9 A. Madder, N. Farcy, N. G. C. Hosten, H. De Muynck, P. J. De Clercq, J. Barry and A. P. Davis, *Eur. J. Org. Chem.*, 1999, 2787–2791.
10 A. J. Nicoll and R. K. Allemann, *Org. Biomol. Chem.*, 2004, **2**, 2175–2180.
11 J. Razkin, H. Nilsson and L. Baltzer, *J. Am. Chem. Soc.*, 2007, **129**, 14752–14758.
12 G. T. Copeland and S. J. Miller, *J. Am. Chem. Soc.*, 2001, **123**, 6496–6502.
13 S. J. Miller, G. T. Copeland, N. Papaioannou, T. E. Horstmann and E. M. Ruel, *J. Am. Chem. Soc.*, 1998, **120**, 1629–1630.
14 C. Schmuck, U. Michels and J. Dudaczek, *Org. Biomol. Chem.*, 2009, **7**, 4362–4368.
15 S. J. Miller, *Acc. Chem. Res.*, 2004, **37**, 601–610.

16 A. Berkessel and D. A. Herault, *Angew. Chem., Int. Ed.*, 1999, **38**, 102–105.
17 A. Furka, F. Sebestyen, M. Asgedom and G. Dibo, *Int. J. Pept. Protein Res.*, 1991, **37**, 487–493.
18 R. A. Houghten, C. Pinilla, S. E. Blondelle, J. R. Appel, C. T. Dooley and J. H. Cuervo, *Nature*, 1991, **354**, 84–86.
19 K. S. Lam, S. E. Salmon, E. M. Hersh, V. J. Hruby, W. M. Kazmierski and R. J. Knapp, *Nature*, 1991, **354**, 82–84.
20 G. W. Cline and S. P. Hanna, *J. Org. Chem.*, 1988, **53**, 3583–3586.
21 M. Blaber, X. J. Zhang and B. W. Matthews, *Science*, 1993, **262**, 917–918.
22 A. Chakrabartty and R. L. Baldwin, *Adv. Protein Chem.*, 1995, **46**, 141–176.
23 A. Chakrabartty, T. Kortemme and R. L. Baldwin, *Protein Sci.*, 1994, **3**, 843–852.
24 P. C. Lyu, M. I. Liff, L. A. Marky and N. R. Kallenbach, *Science*, 1990, **250**, 669–673.
25 J. X. Yang, E. J. Spek, Y. X. Gong, H. X. Zhou and N. R. Kallenbach, *Protein Sci.*, 1997, **6**, 1264–1272.
26 E. J. Spek, C. A. Olson, Z. S. Shi and N. R. Kallenbach, *J. Am. Chem. Soc.*, 1999, **121**, 5571–5572.
27 S. Marqusee, V. H. Robbins and R. L. Baldwin, *Proc. Natl. Acad. Sci. U. S. A.*, 1989, **86**, 5286–5290.
28 A. Kentsis and T. R. Sosnick, *Biochem*, 1998, **37**, 14613–14622.
29 G. R. Marshall, E. E. Hodgkin, D. A. Langs, G. D. Smith, J. Zabrocki and M. T. Leplawy, *Proc. Natl. Acad. Sci. U. S. A.*, 1990, **87**, 487–491.
30 I. L. Karle and P. Balaram, *Biochem*, 1990, **29**, 6747–6756.
31 G. Holzwart and P. Doty, *J. Am. Chem. Soc.*, 1965, **87**, 218–228.
32 C. Toniolo and E. Benedetti, *Trends Biochem. Sci.*, 1991, **16**, 350–353.
33 C. Toniolo, A. Polese, F. Formaggio, M. Crisma and J. Kamphuis, *J. Am. Chem. Soc.*, 1996, **118**, 2744–2745.
34 I. M. Rio-Echevarria, R. Tavano, V. Causin, E. Papini, F. Mancin and A. Moretto, *J. Am. Chem. Soc.*, 2010, **133**, 8–11.
35 B. J. Stapley and A. J. Doig, *J. Mol. Biol.*, 1997, **272**, 465–473.

